Supplementary material

Materials and Methods

Intracellular injections. In general, we followed the method described by Elston and Rosa (1997). The injection apparatus consisted of a fixed stage Olympus BX51W1 microscope equipped with a water immersion long working distance 40x objective, a Leica micromanipulator and a perspex tissue chamber mounted on the stage. Coronal sections (250 μm) were cut with a vibratome and the slices were incubated for 10 min in 10^{-5} M 4,6-diamidino-2-phenylindole (DAPI; Sigma, St. Louis, MO, USA) in 0.1 M phosphate buffer. These DAPI pre-labeled sections were mounted in the injection chamber and the nuclei of cells were visualized UV excitation. This pre-labeling facilitated the impalement of the cell using micropipettes (250–300 MΩ) that were pulled on a Sutter Co. flamming/brown micropipette puller model P-97. Cells were then injected individually with Lucifer Yellow (LY; 8% in 0.1 M Tris buffer, pH 7.4) by hyperpolarizing current in the cytoarchitectonically identified hippocampal formation and the adjacent cortex (including the entorhinal and parahippocampal cortex: **Supplementary Table 1**). LY was applied to each injected cell until the individual dendrites of the cell could be traced to an abrupt end at their distal tips (that fluoresced brightly) and their dendritic spines were readily visible. This fluorescence did not diminish at a distance from the soma, indicating that the dendrites were completely filled. Since intracellular injections of pyramidal cells were made in coronal sections, the part of the dendritic arbor nearer to the surface of the slice from which the cell somata were injected was lost (typically approximately 30 μm from the surface).

Immunohistochemistry

Single immunohistochemistry

Free-floating sections (4-6 sections per case, 50 μm) were pre-treated with 1% H_2O_2 for 30 min to remove the endogenous peroxidase activity and subsequently, the slices used for anti-human Aβ immunochemistry were incubated with 55% formic acid (Sigma-Aldrich, ACS) in PB at room temperature for 20 minutes. All slices were blocked for 1 h in PB with 0.25% Triton-X and 3% normal horse serum (Vector Laboratories Inc., Burlingame, CA, USA). Single immunochemistry was performed with the following monoclonal antibodies: monoclonal mouse anti-human beta-amyloid antibody (Aβ, clone 6F/3D diluted 1:50; Dako, Glostrup, Denmark); mouse anti-human paired helical filaments (PHF)-tau monoclonal antibody (clone AT8, PHF-tau$_{AT8}$; 1:2000, MN1020; Thermo Scientific; Waltham, MA, USA); mouse PHF-1 monoclonal antibody (PHF-tau$_{PHF-1}$; 1:100, kindly supplied by Dr P. Davies: see **Supplementary Figs. 1B-C, 2C-D, G-H**). The PHF-tau$_{AT8}$ antibody has been shown to detect PHF-tau phosphorylated at both Ser202 and Thr205 (Porzig *et al.*, 2007), while PHF-tau$_{PHF-1}$ recognized tau phosphorylated at Ser396 and Ser404 (Greenberg *et al.*, 1992). The sections were incubated overnight at 4°C with the antibodies described above and on the following day, the sections were rinsed and incubated for 2 h with biotinylated horse anti-mouse IgG

antibodies (1:200, BA-2000: Vector Laboratories). After incubating for 1 h in an avidin–biotin peroxidase complex (Vectastain ABC Elite PK6100, Vector), the staining was then finally developed with the 3, 3´ diaminobenzidine tetrahydrochloride chromogen (DAB: Sigma-Aldrich, St. Louis, MO, USA). After staining, the sections were dehydrated, cleared with xylene and coverslipped with DPX (Fluka AG, Buchs, Switzerland). Slices immunostained for Aβ were then counterstained by the Nissl technique (**Supplementary Fig. 1**) to visualize the hippocampal strata or to perform quantitative studies (see below).

Combination of LY intracellular injection with immunohistochemistry and histochemistry

Following intracellular injection of pyramidal neurons with LY, the sections were processed with a rabbit antibody against LY produced at the Cajal Institute [1:400,000 in stock solution containing 2% BSA (A3425, Sigma), 1% Triton X-100 (30632, BDH Chemicals, 5% sucrose in PB] and then with the anti-PHF-tau$_{AT8}$ or anti-PHF-tau$_{PHF-1}$. Antibody binding was detected with a biotinylated donkey anti-rabbit secondary antibody (1:200 in stock solution; RPN1004, Amersham Pharmacia Biotech), followed by a mixture of Alexa fluor 594 anti-mouse (1:1000) and streptavidin coupled to Alexa fluor 488 (1:1000; Molecular Probes, Eugene, OR, USA). Thereafter, the sections were washed in PB and treated with Autofluorescence Eliminator Reagent (2160, Chemicon) to reduce lipofuscin-like autofluorescence without adversely affecting any other fluorescent labelling in the sections. The sections were then washed and mounted with ProLong Gold Antifade Reagent (Invitrogen Corporation, Carlsbad, CA, USA).

After the reconstruction and analysis of the injected cells (see below for details), the slices were recovered and stained for 15 minutes with thioflavin-S in PB to visualize the Aβ plaques (**Supplementary Fig. 4**). The tissue was hydrated in an ethanol series for 5 min at each step (100%, 70%, 50% ethanol and PB), and the sections were again washed in PB and mounted with ProLong Gold Antifade Reagent. Finally, sections containing the selected LY-injected neurons used for quantitative analysis (LY-injected neurons that were immunostained or not for PHF-tau$_{AT8}$ and whose dendrites were not in contact with plaques) were recovered again and processed with the anti-PHF-tau$_{PHF-1}$ following the same protocol described above, in order to check for the presence of PHF-tau$_{PHF-1}$ immunostaining in these injected cells (**Supplementary Fig. 5**).

Quantitative analysis

Estimation of the density and volume occupied by plaques

Two major types of Aβ plaques were observed in the hippocampal formation and adjacent cortex (**Fig. 1B and Supplementary Fig. 1B, F**), diffuse and neuritic plaques (including those with and without an amyloid core: see Garcia-Marin *et al*., 2009). Since layer III of the PHC from patient P9 was injected and the pyramidal cell layer of the CA1 from patients P9, P13 and P14, we calculated the volume occupied by Aβ plaques with respect to the total volume of these layers using unbiased stereology. In the PHC from patient P9, the plaque density was 3,347 plaques/mm^3 and the Aβ plaques occupied an estimated volume of 11%. In the pyramidal layer of CA1, the estimated density of Aβ plaques per mm^3 (DAβ) and the volume they occupied (Vo) varied in the three patients analyzed was: patient P9 - DAβ 423, Vo 9.3%; patient P13 - DAβ 1622, Vo 11.7 %; patient P14 - DAβ 1173, Vo 6.1%. Thus, Aβ plaques occupy a relatively small fraction of layer III in the

PHC of patient P9 and of the CA1 pyramidal layer in the three patients. Although we did not perform a quantitative study on the proportion of the different types of Aβ plaques, most Aβ plaques appeared to be of the diffuse type in layer III of the PHC in patient P9, whereas the majority were neuritic in the CA1 of each patient (**Supplementary Fig. 1 B, F**).

Unbiased stereology was used to quantify and measure the Aβ plaques in five serial Aβ/Nissl sections of the parahippocampal cortex (PHC) and the CA1 from patient P9, and 4-5 Aβ sections in the CA1 from patients P13 and P14. Stereo Investigator software (Microbrightfield, Colchester, VT, USA) was used to drive a motorized stage (Prior Scientific, Houston, TX, USA) on a dual optical head microscope (Olympus BX51) and to mark the plaques at 20x (NA, 0.7) under brightfield optics. The software sequentially chose random counting frames to quantify plaque density in the x, y and z axes (number of plaques/mm^3; 100x100 µm; n= 270 in the PHC from patient P9, and n=1,764, n= 1,883 and n= 1,799 in the CA1 from patients P9, P13 and P14, respectively), moving the motorized stage automatically within the previously defined zones of the PHC and CA1. To obtain homogeneous estimates of Aβ density, tissue shrinkage was evaluated with Stereo Investigator software at five random points of three different sections, estimating shrinkage along the *z* axis in sections after processing for Aβ/Nissl or Aβ staining. The number of labelled plaques was estimated using the optical fractionator method in the Stereo Investigator software and to estimate the plaque volume, the edges of each amyloid plaque were marked with the *Nucleator* probe (Moller *et al.*, 1990). Plaques were only marked if their edges lay within the dissector area and they did not intersect forbidden lines, and if they came into the focus as the optical plane moved through the height of the dissector (10 µm). The guard zone thickness was set to 2-3 µm. This sampling method and the section interval were tested in a pilot experiment to ensure that the estimate of the number of plaques was representative of the total number.

Estimation of the density of PHF-tau$_{AT8}$-ir and PHF-tau$_{PHF1}$-ir neurons

Unbiased stereology was used to quantify the total neuron density (neurons/mm^3), and the neuron density (neurons/mm^3) of PHF-tau$_{AT8}$-ir (immunoreactive) and PHF-tau$_{PHF1}$-ir neurons. We used 4-6 serial sections from the same regions and patients used to estimate the density and volume occupied by the plaques. In addition, the CA3 region was also analyzed in the 3 patients. The Stereo Investigator software (Microbrightfield) was used to drive a motorized stage (Prior Scientific) on a dual optical head microscope (Olympus BX 51) and to mark neurons at 40x (NA, 0.85) under brightfield optics. The software sequentially chose random counting frames to quantify the total neuron density in the x, y and z axes (60x60 µm, n=136 in PHC from patient P9, and n=352, n=294 and n=156 in the CA1 region from patients P9, P13 and P14 respectively; 60x60 µm, n=344, n=228 and n=191 in the CA3 region from P9, P13 and P14 respectively), PHF-tau-$_{AT8}$–ir neuron density (60x60 µm, n=1,458 in the PHC from patient P9, n=800, n=826 and n=781 in CA1 region from patients P9, P13 and P14 respectively) and PHF-tau-$_{PHF1}$–ir neuron density (60x60 µm, n=1,198 in the PHC from patient P9, n=647, n=474 and n=641 in the CA1 region from patients P9, P13 and P14 respectively), moving the motorized stage automatically within the previously delimited zones of the PHC, CA1 and CA3. Tissue

shrinkage was evaluated as described above after processing the sections for Nissl and anti-PHF-tau staining, and the number of labelled neurons was estimated using the optical fractionator method in Stereo Investigator, applying the conditions described previously where the height of the dissector was: 9-10 µm for the total neuron, 8-10 PHF-tau$_{AT8}$-ir neuron density, and 7-9 µm for PHF-tau$_{PHF1}$-ir neuron density. The guard zone thickness was set to 2-3 µm for the total neuron, PHF-tau$_{AT8}$-ir neuron density and for PHF-tau$_{PHF1}$-ir neuron density. Again this sampling method and the section interval were tested in a pilot experiment to ensure that the estimate of the number of neurons was representative of the total number.

The total neuron density was estimated by counting nucleoli in 4-6 Nissl stained sections per region (CA1 and CA3). Neurons with more than one nucleolus were rare but in such cases, only one nucleolus was considered. In the case of PHF-tau$_{AT8}$-ir neurons, we analyzed 6 anti-PHF-tau$_{AT8}$ Nissl counterstained sections in the PHC and CA1 from patient P9, and 5 anti-PHF-tau$_{AT8}$ sections in patients P13 and P14 (**Figure 2**). The density of CA3 neurons in patient P9 was 14,350 neurons/mm^3, whereas in patients P13 and P14 there were only 8,916neurons/mm^3 and 8,447neurons/mm^3. In the case of PHF-tau$_{PHF1}$-ir neurons we analyzed 4 anti-PHF-tau$_{PHF1}$ stained sections per region. In all cases, the density obtained was in reference to the total volume estimated in each region (**Figure 2**).

Reconstruction and morphometric analysis of pyramidal neurons labelled with LY

Imaging was performed with the same confocal laser scanning system described above, again recording Alexa 488 and 594 fluorescence through separate channels. We obtained image stacks of 10-100 image planes (voxel size, 0.057 x 0.057 x 0.28 µm and area 58.36 x 58.36 µm) with a 63x oil-immersion lens (NA, 1.40; refraction index 1.45) using a calculated optimal zoom factor of 2.3. For each stack, the laser intensity and detector sensitivity were set so that the fluorescence signal from the dendritic spines occupied the full dynamic range of the detector. Therefore, some pixels were saturated in the dendritic shaft, but no pixels were saturated within the dendritic spines. After acquisition, the stacks were opened with three-dimensional image processing software, Imaris 7.1 (Bitplane AG, Zurich, Switzerland), the stacks containing images of intracellular injections (green) and PHF-tau$_{AT8}$ staining (red). The red channel was hidden and the stacks were coded (codes that were not broken until the quantitative analysis had been completed). Thereafter, we distinguished two main types of LY-injected neurons: neurons free of PHF-tau$_{AT8}$ somatic staining and neurons with PHF-tau$_{AT8}$ somatic staining (PHF-tau$_{AT8}$-ir neurons). Dendritic parameters were measured by another investigator using the same software but only the green channel to ensure impartiality.

Dendrite diameter was calculated in three dimensions every 10 µm from the soma to the end of the dendrite. *The density of the dendritic spines* was established as the number of dendritic spines found in segments of 10 µm along the length of the dendrite. *Spine volume* was estimated using a method described in detail elsewhere (Benavides-Piccione *et al.*, 2012). Briefly, 7-10 different intensity threshold surfaces were created for each stack of images, and the solid surface that exactly matched the contour of each dendritic spine was then selected. Each dendrite was rotated in 3D and examined to assure that the

solid surface selected for each dendritic spine was appropriate. *The length of dendritic spines* was measured individually, from the point of insertion at the dendritic shaft to the distal tip of the spine while rotating the image in 3D.

References

Benavides-Piccione R, Fernaud-Espinosa I, Robles V, Yuste R, DeFelipe J (2012) Age-Based Comparison of Human Dendritic Spine Structure Using Complete Three-Dimensional Reconstructions. Cereb Cortex. 2012 Jun 17.

Elston GN, Rosa MG. The occipitoparietal pathway of the macaque monkey: comparison of pyramidal cell morphology in layer III of functionally related cortical visual areas. Cereb Cortex. 1997; 7:432-452.

Porzig R, Singer D, Hoffmann R. Epitope mapping of mAbs AT8 and Tau5 directed against hyperphosphorylated regions of the human tau protein. *Biochem Biophys Res Commun* 2007; 358:644-649.

Garcia-Marin V, Blazquez-Llorca L, Rodriguez JR, Boluda S, Muntane G, Ferrer I et al. Diminished perisomatic GABAergic terminals on cortical neurons adjacent to amyloid plaques. Front. Neuroanat 2009; 3:28.

Greenberg SG, Davies P, Schein JD, Binder LI. Hydrofluoric acid-treated tau PHF proteins display the same biochemical properties as normal tau. *J Biol Chem* 1992; 267:564-569.

Moller A, Strange P, Gundersen HJ. Efficient estimation of cell volume and number using the nucleator and the disector. *J Microsc* 1990; 159:61-71.

Patient	P9	P11	P12	P13	P14
Age/Gender	Male/82	Male/75	Female/82	Male/83	Female/87
NF/Aβ pathology Braak stage	AD V/C	ADIII/B and AGD	AD V/C and LB	AD VI/C and LB	AD III-IV /0-A
Postmortem delay (h)	3	2:30	2	2:30	1:30
Cause of death	Bronchopneu-monia plus heart failure	Lymphoproli-ferative disorder	Heart failure	Respiratoy failure	Respiratoy infection
Cortical regions and number of LY-injected neurons					
CA1	40 (15)	19	71	62 (8)	48 (8)
CA2	-	-	7	15	-
CA3	-	-	35	40	47
GD	-	-	-	-	37
Subiculum	14	-	-	-	-
Enthorrinal cortex	-	37	67	-	-
Parahippocampal cortex	96 (11)	-	-	69	-

Supplementary Table 1. Summary of the patient data and the LY-injected neurons in each cortical area and patient. In brackets are indicated the number of neurons used for 3D examination. Aβ, Amyloid-β; AGD, Argyrophilic, grain disease; LB, Lewy bodies; NF, Neurofibrillar.

Patient	*Region*	*PHF immunostaining*	*Dendrite diameter (µm)*	*Spine density (spines/µm)*	*Spine length (µm)*	*Spine volume ($µm^3$)*
P9	**PHC**	PHF-tau$^-$	0.949 ± 0.039	1.256 ± 0.105	1.442 ± 0.051	0.330 ± 0.019
		PHF-tau$^+$	0.961 ± 0.025	1.278 ± 0.125	1.499 ± 0.044	0.332 ± 0.019
		P	>0.05	>0.05	>0.05	>0.05
	CA1	PHF-tau$^-$	1.197 ± 0.075	1.881 ± 0.189	1.005 ± 0.036	0.307 ± 0.054
		PHF-tau$^+$	0.954 ± 0.021	1.610 ± 0.155	0.858 ± 0.026	0.223 ± 0.014
		P	0.024	>0.05	0.016	>0.05
P13	**CA1**	PHF-tau$^-$	0.938 ± 0.061	2.139 ± 0.177	1.173 ± 0.142	0.250 ± 0.068
		PHF-tau$^+$	0.814 ± 0.053	1.589 ± 0.095	1.164 ± 0.015	0.264 ± 0.064
		P	>0.05	0.029	>0.05	>0.05
P14	**CA1**	PHF-tau$^-$	0.940 ± 0.073	2.674 ± 0.221	0.988 ± 0.029	0.216 ± 0.023
		PHF-tau$^+$	0.805 ± 0.091	1.772 ± 0.085	1.063 ± 0.032	0.243 ± 0.026
		P	>0.05	0.009	>0.05	>0.05

Supplementary Table 2. Summary of the statistical analysis of dendrite diameter, spine density, spine length and spine volume, showing the average (mean ± SEM) and P value in each cortical area (parahippocampal cortex –PHC and CA1) and AD patient (P9, P13 and P14), indicating the values of PHF-tau$^-$ and PHF-tau$^+$ neurons. PHF-tau$^-$; neurons no immunostained for PHF-tau$_{AT8}$ and PHF-tau$_{PHF\text{-}1}$. PHF-tau$^+$; neurons immunostained for PHF-tau$_{AT8}$ and PHF-tau$_{PHF\text{-}1}$.

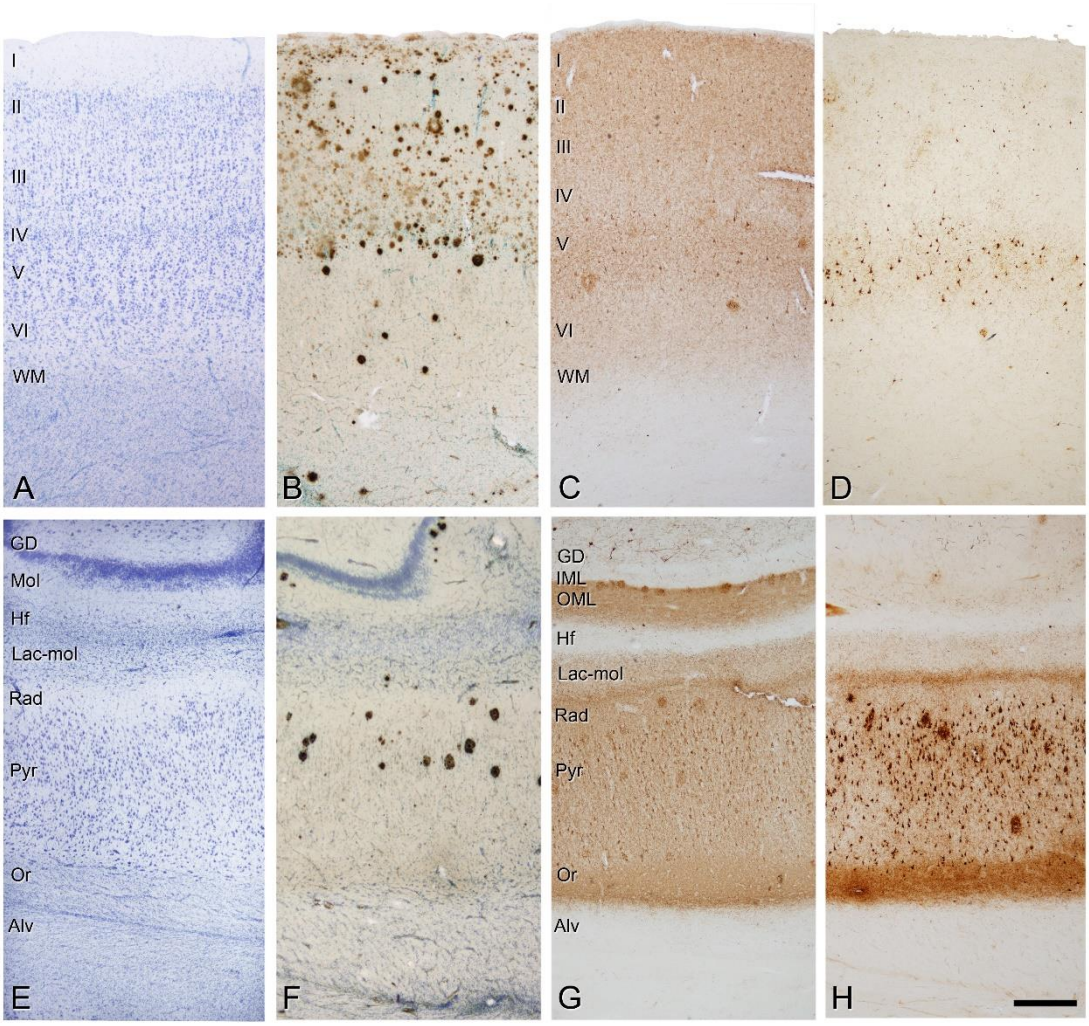

Supplementary Figure 1
A and **E**, **B** and **F**, **C** and **G**, and **D** and **H**, higher magnification of the sections shown in **Figures 1A**, **1B**, **1C** and **1D**, respectively. Nissl (**A, E**), Aβ/Nissl (**B, F**), PHF-tau$_{AT8}$ (**C, G)** and PHF-tau$_{PHF-1}$ (**D, H**) stained sections from the PHC (**A**-**D**) and CA1 (**E**-**H**) region. Alv, alveus; DG, dentate gyrus; Hf, hippocampal fissure; IML, inner molecular layer; Lac-mol, stratum lacunosum-moleculare; Mol, molecular layer; OML, outer molecular layer; Or, stratum oriens; Pyr, stratum pyramidale Rad, stratum radiatum; WM, white matter; Scale bar (in **H**): 250 µm in **A**-**H**.

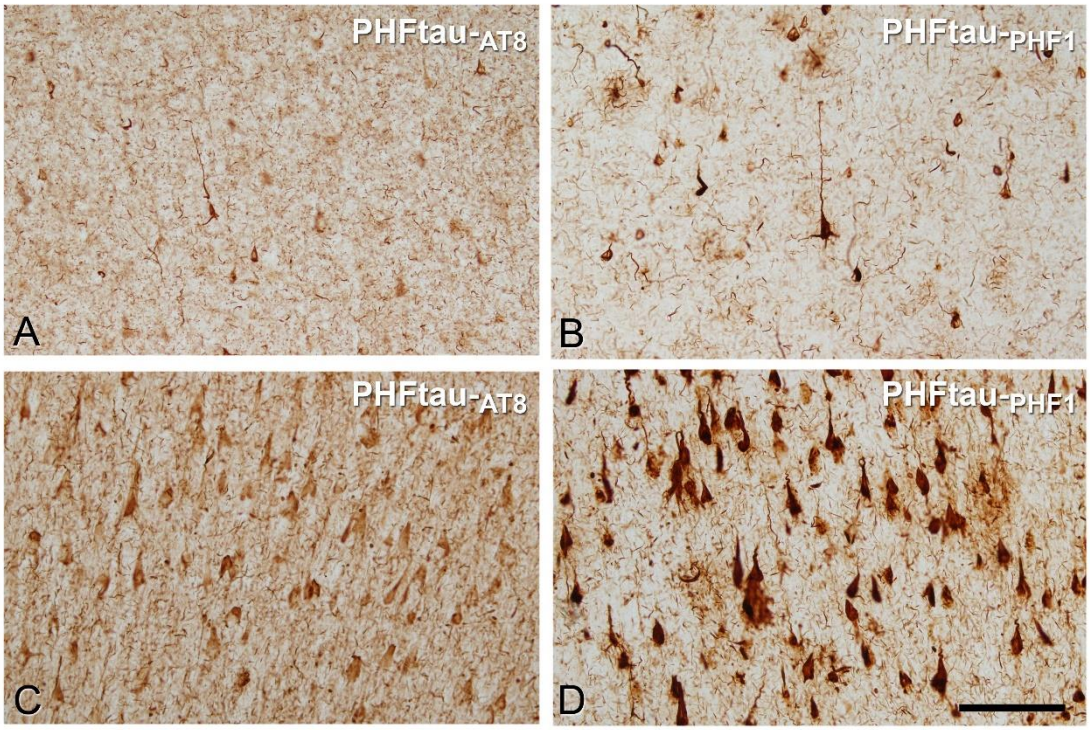

Supplementary Figure 2
A, **C** and **B**, **D** higher magnification of **Figures 1C** and **1D**, respectively, to illustrate the immunostaining for PHF-tau$_{AT8}$ and PHF-tau$_{PHF-1}$ in layer III of the PHC (**A**, **B**) and the pyramidal cell layer of CA1 (**C**, **D**). Scale bar (in **D**): 170 µm in **A-D**.

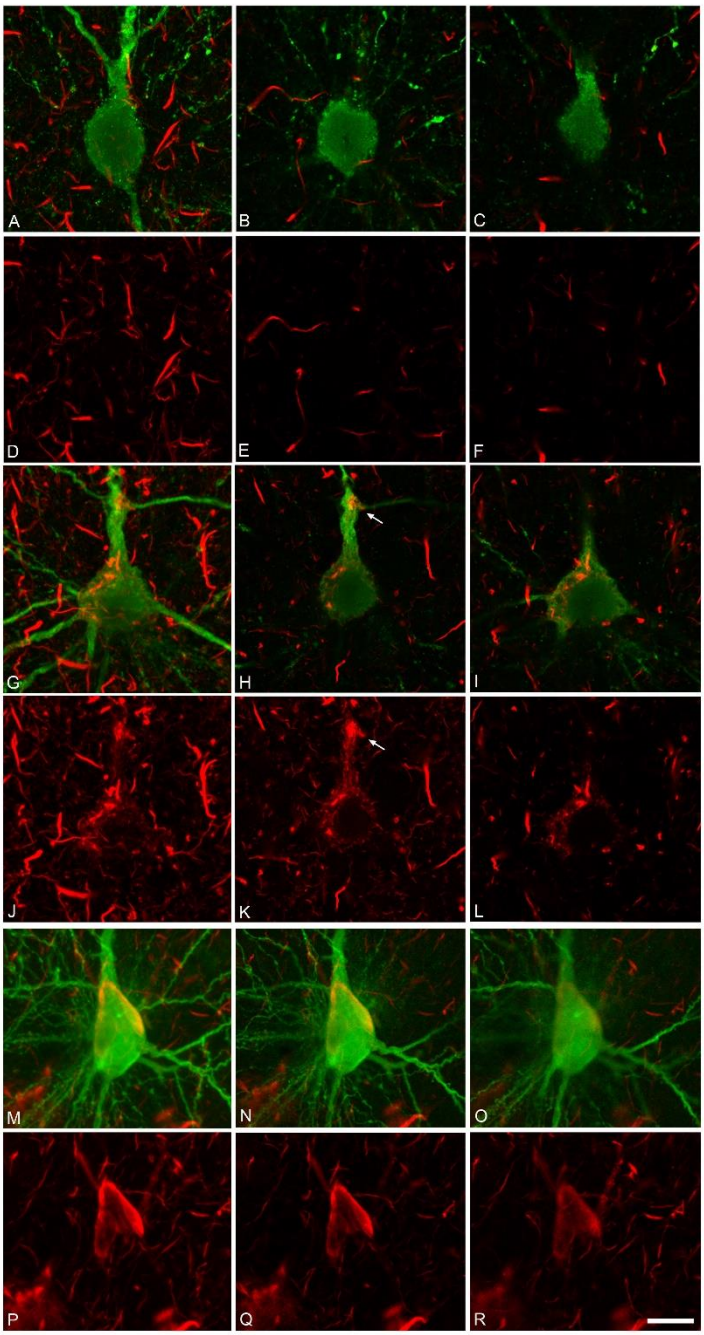

Supplementary Figure 3
Combined intracellular LY injection (green) and PHF-tau$_{AT8}$ (red) immunohistochemistry showing a higher magnification of the cell bodies of LY-injected pyramidal neurons from **Figures 4B** (**A**-**F**; PHF-tau$_{AT8}^{-}$) and **4H** (**G**-**L**; PHF-tau$_{AT8}^{+}$ pattern I) and from a PHF-tau$_{AT8}^{+}$ neuron with pattern IIa (**M**-**R**). **A**, **D**, Stack of 16 confocal sections showing the soma of a LY labelled neuron no immunostained for PHF-tau$_{AT8}$ after combining the red and green channels (**A**), or showing the red channel alone (**D**). **B**, **C**, **E**, **F**, Single optical sections from the stack shown in **A**. **G**, **J**, Stack of 22 confocal optical sections showing the soma of the labelled PHF-tau$_{AT8}$–ir LY neuron with pattern I after combining the red and green channels (**G**), or displaying the red channel alone (**J**). **H**, **I**, **K**, **L**, Single optical sections from the stack shown in **G**. Note the accumulation of PHF-tau$_{AT8}$-ir aggregates in the initial proximal segment of the apical dendrite (arrow) of the injected cell. **M**, **P**, Stack of 21 confocal optical sections showing the soma of a labelled PHF-tau$_{AT8}$–ir LY neuron with pattern IIa after combining the red and green channels (**M**), or displaying the red channel alone (**P**). **N**, **O**, **Q**, **R**, Individual optical sections from the stack shown in **M**. Scale bar (in **R**): 10 µm in **A**-**R**.

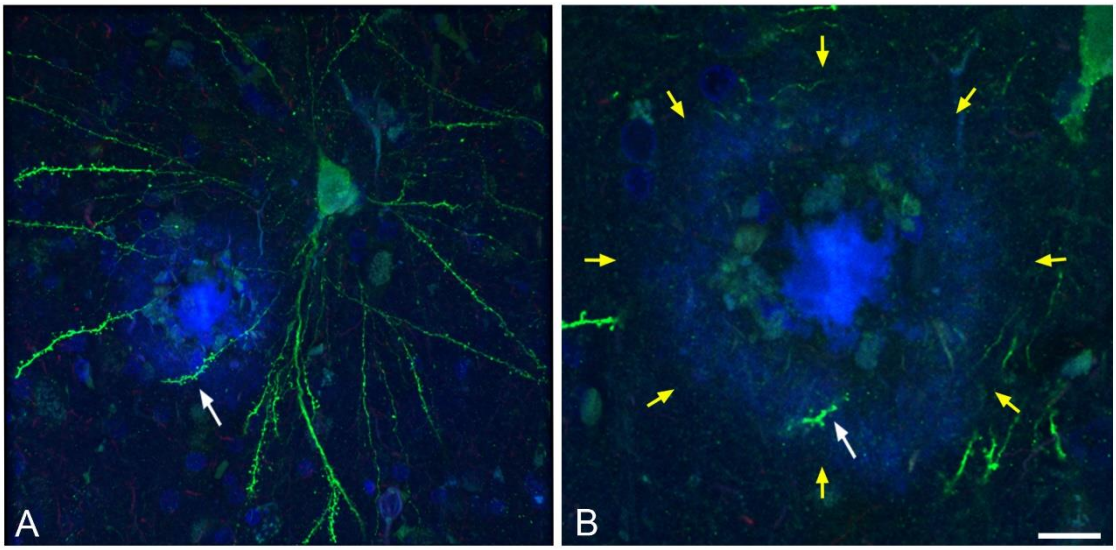

Supplementary Figure 4
Method used to identify the dendrites of intracellularly labelled cells in contact with Aβ plaques. **A**, Confocal microscopy image of a LY-injected neuron from layer III of the PHC from patient P9 stained with thioflavin-S to visualize the Aβ plaques. The white arrow shows a dendrite in contact with a plaque (blue). **B**, Higher magnification of **A** in a single optical section to show that the labelled dendrite lies within the periphery (yellow arrows) of the Aβ plaque. Scale bar (in **B**): 20 µm in **A**; and 10 µm in **B**.

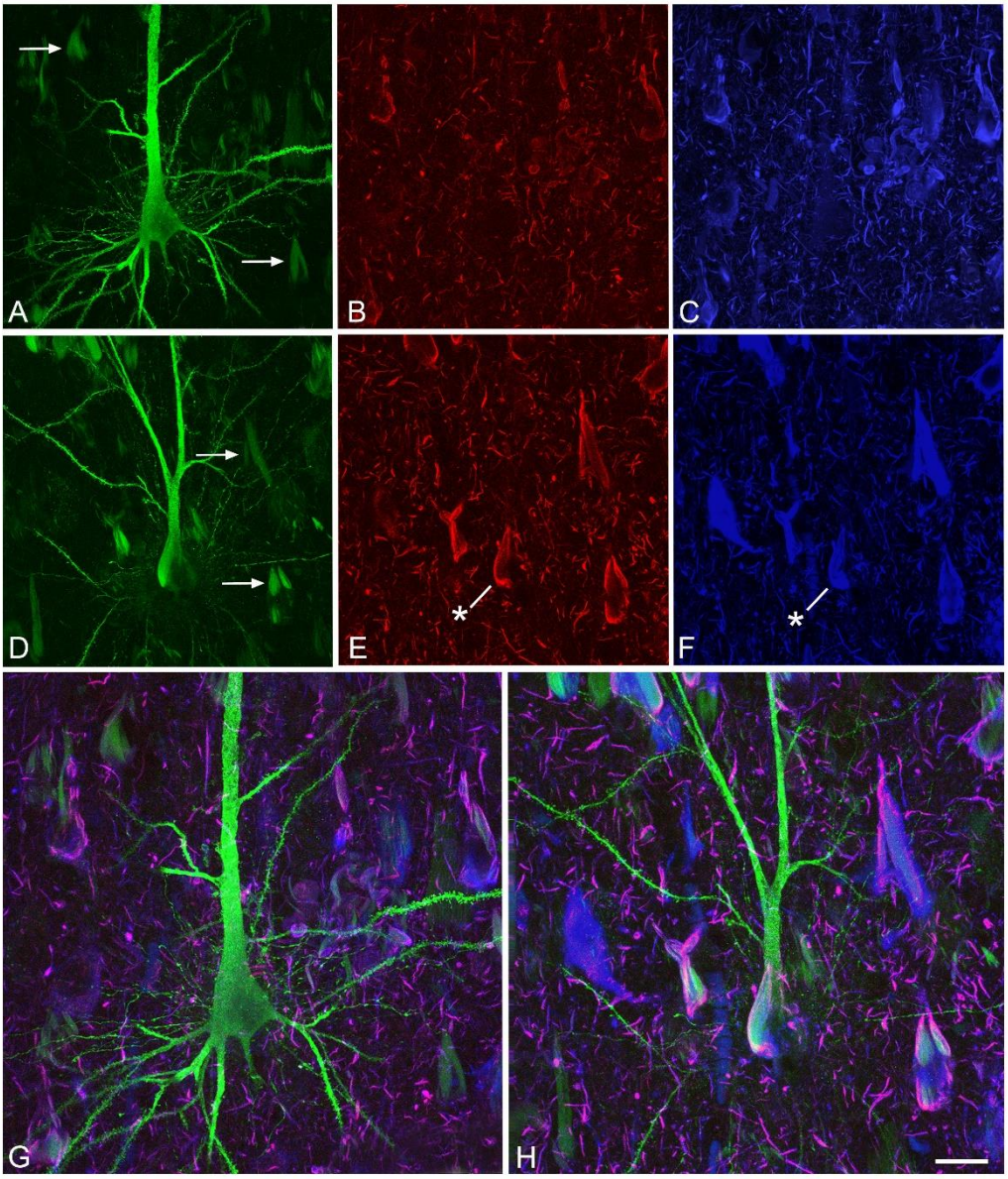

Supplementary Figure 5. (A-H) Combined intracellular LY injection and thioflavin S (green) and PHF-tau$_{AT8}$ (red) and PHF-tau$_{PHF-1}$ (pseudocolored in blue) immunohistochemistry showing a LY neuron that was not labeled for PHF-tau$_{AT8}$ or PHF-tau$_{PHF-1}$ **(A-C)** and a double-labeled LY neuron for PHF-tau$_{AT8}$ and PHF-tau$_{PHF-1}$ **(D-F)** (asterisks). These two neurons are also shown in **Fig. 5 B** and **G**, respectively. Arrows in **A** and **D** indicate some thioflavin S positive neurons. **G**, **H**, images obtained after combining the channels acquired separately in **A**-**C** and **D**-**F**, respectively. Neurons that are labeled for both PHF-tau$_{AT8}$ and PHF-tau$_{PHF-1}$ are visualized with a purple color. Note that the labeling of neurons for both PHF-tau$_{AT8}$ and PHF-tau$_{PHF-1}$ could be due to antibody cross-reactivity (see text for further details). Scale bar (in **H**): 30 μm in **A**-**F**; 17 μm in **G**, **H.**

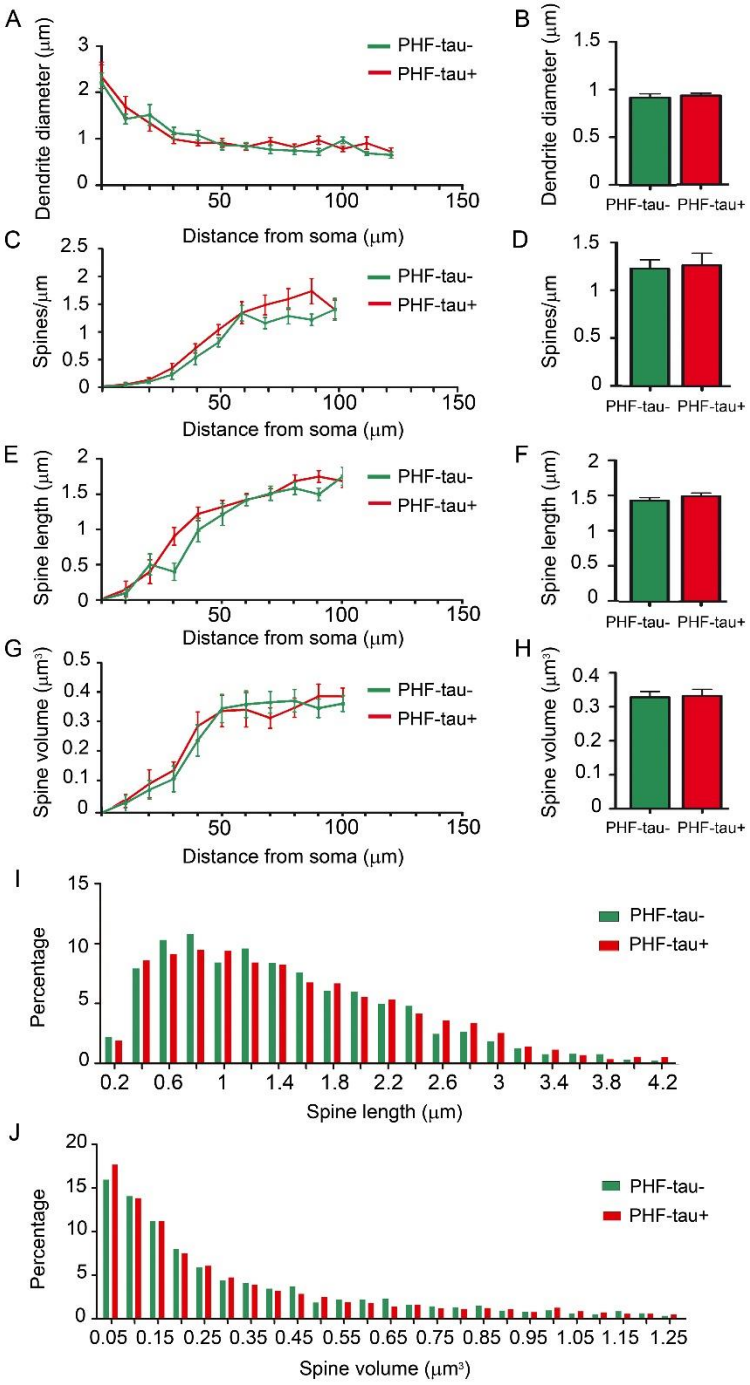

Supplementary Figure 6

Comparative morphometric analysis of dendrites from LY-injected PHF-tau^{+} pyramidal neurons and dendrites from LY-injected PHF-tau^{-} neurons in layer III of the PHC. **A**, Dendrite diameter in function of the distance from soma. **B**, Average diameter per dendrite. **C**, Dendritic spine density (dendritic spines/µm) in function of the distance from the soma. **D**, Average spine density per dendrite. **E**, Dendritic spine length in function of the distance from soma. **F,** Average dendritic spine length per dendrite. **G**, Dendritic spine volume in function of the distance from soma. **H**, Average dendritic spine volume per dendrite. **I**, **J**, Frequency distribution of dendritic spine lengths (**I**) and volumes (**J**). No significant changes were observed for any of the morphometric parameters analysed in the PHC (two way ANOVA, Bonferroni *post-hoc*, *P>0.05* - **A**, **C**, **E**, **G**); *Mann-Whitney* test, *P>0.05* - **B**, **D**, **F**, **H**); Kolmogorov-Smirnov *P>0.05* - I, J).

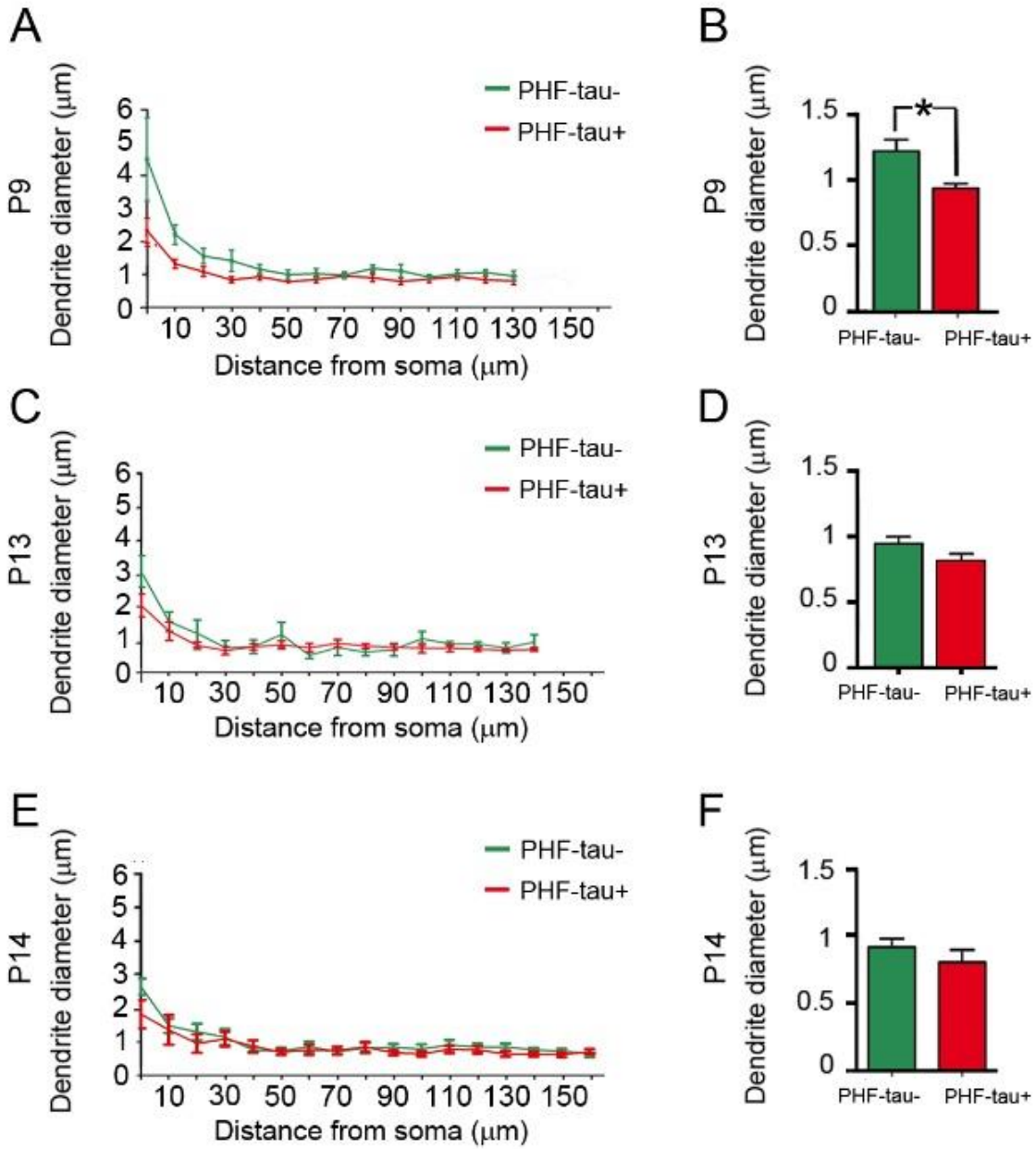

Supplementary Figure 7
Comparative morphometric analysis of dendrite diameter of LY-injected PHF-tau$^+$pyramidal neurons and dendrites from LY-injected PHF-tau$^-$ neurons in the CA1 of patient P9 (**A-B**), patient P13 (**C**, **D**) and patient P14 (**E**, **F**). **A**, **C**, **E**, Dendrite diameter in function of the distance from soma. **B**, **D**, **F**, Average dendritic diameter per dendrite. Significant differences were found for the morphometric parameters shown in **B** (*Mann-Whitney* test, **P<0.05)* and **E** (two way ANOVA, Bonferroni *post-hoc*, *, $P < 0.05$).

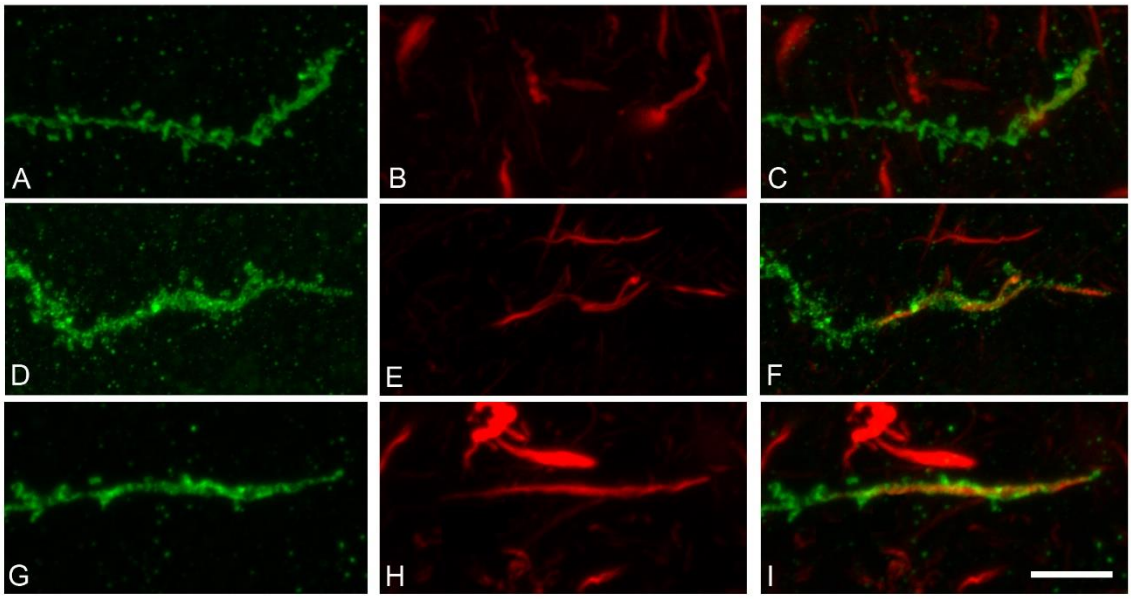

Supplementary Figure 8
Combination of LY intracellular injection (green) and PHF-tau$_{AT8}$ immunohistochemistry (red) in the CA1. Stacks of 18-21 optical confocal sections showing distal dendrites from three PHF-tau$_{AT8}$-ir neurons (pattern IIa immunostaining) (**A**, **D**, **G**) that contained fibrillar PHF-tau$_{AT8}$ aggregates (**B**, **E**, **H)**. **C**, **F**, **I**, Images obtained by combining the red and green channels from the confocal microscope. Note the low density of dendritic spines in the distal segments (see **Supplementary Fig. 9**). Scale bar (in **I**): 4 µm in **A-I**.

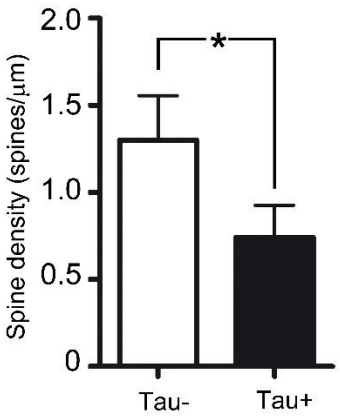

Supplementary Figure 9
Graph showing the dendritic spine density in the distal segments (10-20 µm) of dendrites containing fibrillar PHF-tau$_{AT8}$ (Tau+) and in the adjacent segments of the same length (pre-terminal segments lacking PHF-tau$_{AT8}$:Tau-). *, $P < 0.05$; *Mann-Whitney* test.